HHS Public Access

Author manuscript

Biosens Bioelectron. Author manuscript; available in PMC 2024 March 15.

Published in final edited form as:

Biosens Bioelectron. 2023 March 15; 224: 115030. doi:10.1016/j.bios.2022.115030.

A tissue chip with integrated digital immunosensors: In situ brain endothelial barrier cytokine secretion monitoring

Shiuan-Haur Su[a], **Yujing Song**[a], **Andrew Stephens**[a], **Muyu Situ**[e], **Molly C. McCloskey**[g], **James L. McGrath**[g], **Anuska V. Andjelkovic**[f], **Benjamin H. Singer**[c,d,**], **Katsuo Kurabayashi**[a,b,d,*]

[a]Department of Mechanical Engineering, University of Michigan, Ann Arbor, MI, 48109, USA

[b]Department of Electrical Engineering and Computer Science, University of Michigan, Ann Arbor, MI, 48109, USA

[c]Department of Internal Medicine, Division of Pulmonary and Critical Care Medicine, University of Michigan, Ann Arbor, MI, 48109, USA

[d]Weil Institute for Critical Care Research and Innovation, University of Michigan, Ann Arbor, MI, 48109, USA

[e]Neuroscience Graduate Program, University of Michigan, Ann Arbor, MI, 48109, USA

[f]Department of Pathology and Neurosurgery, University of Michigan, Ann Arbor, MI, 48109, USA

[g]Department of Biomedical Engineering, University of Rochester, Rochester, NY, 14627, USA

Abstract

Organ-on-a-chip platforms have potential to offer more cost-effective, ethical, and human-resembling models than animal models for disease study and drug discovery. Particularly, the Blood-Brain-Barrier-on-a-chip (BBB-oC) has emerged as a promising tool to investigate several neurological disorders since it promises to provide a model of the multifunctional tissue working as an important node to control pathogen entry, drug delivery and neuroinflammation. A comprehensive understanding of the multiple physiological functions of the tissue model requires biosensors detecting several tissue-secreted substances in a BBB-oC system. However,

[*]Corresponding author. Department of Mechanical Engineering, University of Michigan, Ann Arbor, MI, 48109, USA. katsuo@umich.edu (K. Kurabayashi). [**]Corresponding author. Department of Mechanical Engineering, University of Michigan, 2350 Hayward St, Ann Arbor, MI, 48109, USA. singerb@med.umich.edu (B.H. Singer).

Author contributions

Shiuan-Haur Su: Conceptualization, Investigation, Methodology, Software, Writing- Original draft preparation. **Yujing Song:** Conceptualization, Software, Resources, Validation. **Andrew Stephens:** Resources, Validation. **Muyu Situ:** Resources, Investigation. **Molly C. McCloskey:** Resources. **James McGrath**: Funding Acquisition, Resources, Writing - Review & Editing. **Anuska V. Andjelkovic:** Resources, Writing - Review & Editing. **Benjamin H. Singer:** Conceptualization, Methodology, Funding Acquisition, Writing - Review & Editing, Supervision. **Katsuo Kurabayashi:** Conceptualization, Methodology, Funding Acquisition, Writing - Review & Editing, Supervision.

Declaration of competing interest

The authors declare the following financial interests/personal relationships which may be considered as potential competing interests: J. L.M. is a cofounder of SiMPore and holds an equity interest in the company. SiMPore is commercializing ultrathin silicon-based technologies including the membranes used in this study. A U.S. provisional patent was filed for the digital immunosensor technology employed in the assay reported in the manuscript under Application No 63/016,753 on April 28, 2020.

Appendix A. Supplementary data

Supplementary data to this article can be found online at https://doi.org/10.1016/j.bios.2022.115030.

current sensor-integrated BBB-oC platforms are only available for tissue membrane integrity characterization based on permeability measurement. Protein secretory pathways are closely associated with the tissue's various diseased conditions. At present, no biosensor-integrated BBB-oC platform exists that permits in situ tissue protein secretion analysis over time, which prohibits researchers from fully understanding the time-evolving pathology of a tissue barrier. Herein, the authors present a platform named "Digital Tissue-BArrier-CytoKine-counting-on-a-chip (DigiTACK)," which integrates digital immunosensors into a tissue chip system and demonstrates on-chip multiplexed, ultrasensitive, longitudinal cytokine secretion profiling of cultured brain endothelial barrier tissues. The integrated digital sensors utilize a novel beadless microwell format to perform an ultrafast "digital fingerprinting" of the analytes while achieving a low limit of detection (LoD) around 100–500 fg/mL for mouse MCP1 (CCL2), IL-6 and KC (CXCL1). The DigiTACK platform is extensively applicable to profile temporal cytokine secretion of other barrier-related organ-on-a-chip systems and can provide new insight into the secretory dynamics of the BBB by sequentially controlled experiments.

Keywords

Organ-on-a-chip; Tissue chip; Blood-brain-barrier; Cytokine secretion; Digital immunoassay; Multiplex biomarker detection

1. Introduction

Recent advances in Organ-on-a-chip (OoC) or tissue chip technology have enabled researchers to create engineered or natural tissues within microfluidic chips. Much promise arises in observing the tissues' physiological phenomena under conditions replicating complex in vivo biological environments (Low et al., 2021). Animal models are the current gold standard for preclinical validation of therapeutics. However, animal studies require breeding, dissections, and ethical clearances. Preclinical studies in the U.S. use as many as 111 million mice every year (Carbone, 2021), which is a huge cost to the biomedical research and drug discovery industry. More importantly, cross-species differences between animals and humans have failed many animal studies attempting to develop a therapy for the human central nervous system (CNS). Replacing animal models with OoC platforms may eliminate these issues and provide accessibility and throughput for blood brain barrier (BBB) studies. The BBB is a highly selective vascular border of the CNS with complex functions, including transporting metabolic products, preventing crossing of bloodborne pathogens and neurotoxic substances, and regulating immune responses on the fragile abluminal side (Obermeier et al., 2013). One of the OoC subsets, BBB-on-a-chip (BBB-oC), facilitates BBB-penetrable drug discovery or studies of CNS disease mechanisms (Oddo et al., 2019). Researchers have studied the integrity of the barrier during BBB-oC experiments with integrated sensors (Ahn et al., 2020; Badiola-Mateos et al., 2021; Yu et al., 2020). However, these studies have been limited to using trans-endothelial electrical resistance (TEER) sensors to characterize membrane permeability and integrity (Liang and Yoon, 2021; Mir et al., 2022; Wolff et al., 2015). The electrophysical measurements only provide a nonspecific signature of the membrane functionality, masking multiple combined biological factors. The research community foresees the tremendous scientific impact of

longitudinally monitoring markers other than permeability in a BBB-oC, such as tissue-secreted neuroinflammatory cytokines, since they provide a clearer picture of the dynamic change of tissue physiology over time in CNS investigations (Larochelle et al., 2011; Liang and Yoon, 2021; Lv et al., 2010; Mir et al., 2022). Establishing such an ability calls for immunosensors detecting tissue- or cell-secreted proteins.

Immunosensors previously integrated into other OoC systems include localized surface plasmon resonance (LSPR) sensors for adipose tissue (Zhu et al., 2018) and electrochemical sensors for heart, liver organoids and muscle tissues (Ortega et al., 2019; Zhang et al., 2017). However, the poor linear range of these sensors (Zhang and Noji, 2017) limits their direct implementation in BBB-oC immunosensing. An ideal BBB-oC experiment necessitates a high throughput platform integrated with multiplexed, sensitive immunosensors achieving large dynamic ranges. The BBB-oC should allow us to measure low-abundance neurotoxicity-inducing biomarkers, such as cytokines, and monitor multiple time-varying protein secretion behaviors of the BBB model. The synthesis and release of cytokines are highly regulated and temporally orchestrated in the immune system (Lacy and Stow, 2011). Through positive feedback, inflammatory cytokines induce a self-perpetuating cascade that synergistically upregulates other inflammation biomarkers like chemokines and cell adhesion molecules (CAMs) (Lecuyer et al., 2016; Lombardi et al., 2009). However, the mere presence of some inflammatory chemokines like MCP1 (or CCL2) may not indicate neuroinflammation but offer neuroprotective functions to the BBB (Schilling et al., 2009; Stowe et al., 2012; Williams et al., 2014). Thus, temporal monitoring of the homeostatic BBB cytokine levels, immune cascade onset, progression, and resolution can provide critical information such as the “tipping point” to sustained chronic neuroinflammation and the true physiological picture (DiSabato et al., 2016; Gilroy and Lawrence, 2008). This information can be obtained through multiple endpoint measurements in some situations. But at the same time, these measurements require time, materials, and sample resources and introduce additional batch effects that decrease reproducibility. Achieving a high throughput assay can suppress cellular batch effects and mitigate the long sample preparation time usually accompanying BBB cell culture preparation and induced pluripotent stem cells (iPSC)-related applications. Unfortunately, conventional immunosensors fail to meet these needs as they cannot detect a subtle concentration change of low abundance analytes or achieve multiplex capabilities for a panel of markers co-existing in highly different concentration ranges. As a result, a BBB-oC experiment with these immunosensors cannot trace rare biomarkers or probe the tissue’s abrupt, temporally resolved secretory responses. Furthermore, integrating these immunosensors often requires complex fluidic circuits, making the BBB-oC platform inaccessible to non-engineering labs.

Herein, we present a new class of immunosensor-integrated platform for tissue barrier studies named “**Digi**tal **T**issue-B**A**rrier-**C**yto**K**ine-counting-on-a-chip (DigiTACK)” to fill the technology gap above. In this work, DigiTACK models a brain endothelial cell layer representing the barrier between the luminal (blood) and abluminal (brain) sides of the brain microvasculature that is subjected to endotoxin (LPS) exposure. The device detects a panel of three cytokine species relevant to neuroinflammation (Fig. 1A). DigiTACK combines the modular μSIM platform (McCloskey et al., 2022) with an improved version

of our previously reported single molecule-counting digital immunosensors (Song et al. 2020, 2021a, 2021b; Su et al., 2021) (Fig. 1B). The μSIM tissue chip platform features a highly permeable, bio-resembling ultrathin nanoporous silicon-nitride (NPN) membrane with transparency for optical imaging. Its stacked configuration (Mir et al., 2022) offers modularity and scalability and has demonstrated multiple applications in studying the BBB (Castro Dias et al., 2021; Hudecz et al., 2020; Mansouri et al., 2022; McCloskey et al., 2022; Mossu et al., 2019; Salminen et al., 2020). The integrated digital immunosensors have a multiplexed cytokine detection capability with a short incubation/detection time (<15 min) and a very low limit of detection (LoD) (~100–500 fg/mL). Each immunosensor only utilizes <0.1% of molecules in bulk solution to generate digital sensor signals, minimally affecting the analyte concentration in the original media during in situ measurements. All together, these immunosensor features enable us to perform in situ longitudinal cytokine secretion profiling for MCP1, IL-6 and KC (or CXCL1) on both luminal and abluminal sides across a mouse brain microvascular endothelial cells (mBMEC) barrier formed on the DigiTACK chip. (Fig. 2). Stimulating the mBMEC barrier with endotoxin, we observed significant asymmetry in the cytokine secretion behavior of the layer between the luminal and abluminal sides and distinct, characteristic patterns with the temporal profiles across the three cytokines. These interesting observations highlight that the DigiTACK platform promises to pave the way for developing new drug screening, disease mechanism exploration, and pharmacological therapy methods.

2. Material and methods

2.1. DigiTACK component 1 and component 1 strip preparation

Component 1 is a modified version of the modular μSIM (McCloskey et al., 2022) which consists of a nanoporous silicon nitride (NPN) membrane chip (SiMPore Inc., USA) (Fig. 1B(iii)), an acrylic membrane housing block (ALine Inc., USA), a through cut double-sided silicon-based pressure sensitive adhesive (PSA, ALine Inc., USA) and a through-cut Polydimethylsiloxane (PDMS) (DOW SYLGARD™ 184, Dow chemical, USA) thin film channel (Fig. 1B(i)). Details of the fabrication of the NPN membrane and acrylic membrane housing block as well as the assembly of these two parts can be found in a previously reported work (McCloskey et al., 2022). The PDMS thin-film channel layer was first prepared by spin coating uncured PDMS (curing agent to base ratio 1:10) on an acrylic substrate, curing it at 60 °C, laser cutting both materials, then releasing the PDMS thin film channel from the acrylic substrate. Double-sided PSA layers with the same geometry as the PDMS thin film channels were also mass produced by laser cutting. We later irreversibly bonded the PDMS thin-film channel layer to the bottom of each acrylic housing block via the double-sided PSA layer. Multiple Component 1 units were assembled into a 2 × 4 arrayed strip-like format termed “Component 1 strip” (Fig. 2A and Fig. S2A) for high-throughput experiments. The open-ended reservoir in the membrane housing block will later be referred to as the “luminal compartment”, and the bottom chamber enclosed by the PDMS thin film channel as the “abluminal compartment”.

2.2. DigiTACK component 2 (beadless digital counting chip) preparation

First, photoresist (MEGAPOSIT™ SPR™220, Dow chemical, USA) was patterned on a fused silica glass wafer using a conventional photolithography technique (Fig. S1(I)). Here, the patterned resist layer later serves as a mask for deep glass reactive ion etching (DGRIE) to etch microwells into the wafer (Figure S1(II)). The wafer was then plasma activated and placed in a chemical vapor deposition (CVD) chamber for vapor phase APTES conjugations (Figure S1(III)). The wafer was then sonicated in acetone for 5 min to remove photoresist and rinsed subsequently with isopropyl alcohol (IPA) and deionized water (DI) to remove acetone (Figure S1(IV)). We then covered the glass wafer with a PDMS coating to create a hydrophobic surface for oil sealing in the downstream digital sensor reading and to prevent liquid residue and leakage when moving Component 1 on top during the longitudinal assay. A PDMS layer with microfluidic channels (PDMS microfluidic channel layer) was then attached to the wafer to perform micropatterning and conjugation of capture antibodies. Then, a microfluidic spatial encoding method was applied to perform multiplexed digital assays in which a specific location was registered for the signal of a specific marker as used in our previous studies (Song et al. 2021a, 2021b; Su et al., 2021). MCP1 (#505901, BioLegend, USA), IL-6 (#504501 BioLegend, USA), KC (#DY453-05, Bio-Techne, USA) capture antibodies were diluted in Phosphate-buffered saline (PBS) and incubated in designated microfluidic channels overnight. After antibody conjugation to the APTES (Fig. S1(V)), PBS-T (PBS + 0.05% Tween 20) was flowed into the microfluidic channels to remove excess antibodies, and the PDMS microfluidic channel layer was removed. A low residue tape was then pressed on top of the microwells to exfoliate the nonspecifically bound antibodies that could not be removed through liquid phase washing (Figure S1(VI)). These processes yielded a hydrophilic-in-hydrophobic capture-antibody-coated microwell array for digital counting assays as shown in Figure S1(VII). For quality control, we further labelled the capture antibodies (rat-sourced) with Alexa fluor 488 anti-rat-IgG antibodies (#405418, BioLegend, USA) to verify that high-density conjugation of capture antibodies was successfully achieved within the microwells while leaving no antibodies on the microwells' top surfaces. The finished wafer is later referred to as "Component 2" (Fig. S2B).

2.3. Primary mouse brain endothelial cell culture and stimulation in DigiTACK

Primary mouse brain microvascular endothelial cells (mBMEC) (C57BL/6 mouse primary brain microvascular endothelial cells, #C57-6023, Cell Biologics, USA) were cultured in endothelial cell medium (ECM) (#M1168 Complete Mouse Endothelial Cell Medium, Cell Biologics, USA). The mBMECs were seeded onto 0.5% gelatin-coated flasks and cultured in endothelial cell medium (ECM) supplemented with 20% Fetal bovine serum (FBS), 1% antibiotic-antimycotic solution, growth factors cocktails (VEGF, ECGF and EGF), hydrocortisone and heparin (#M1168 Complete Mouse Endothelial Cell Medium, Cell Biologics, USA) at 37 °C and 5% CO2 in humid atmosphere.

In the cell preparation phase of the experiment, a Component 1 strip was first attached and sealed to a glass surface without digital sensor patches. The NPN membranes in the Component 1 strip were first coated with a gelatin-based coating buffer (#6950 Gelatin-Based Coating Solution, Cell Biologics, USA) for >30 min at 37 °C. Then, we plate 100

μL of cell suspension at concentrations 1.4×10^5 cells/mL onto the NPN membrane in the luminal compartment of each device (~480 cells/mm^2) and fill the abluminal compartment with just the ECM. The devices are then incubated in a moisture controlled, 37 °C, 5% CO2 incubator. We replaced culture medium every other day with preheated ECM. The cultured mBMEC usually formed tight junctions within 3–4 days post-plating and became ready for endotoxin stimulation in the DigiTACK assay. For the stimulated groups, we dispensed freshly prepared and prewarmed LPS (500 ng/mL) in high glucose Dulbecco's Modified Eagle Medium (DMEM) into the luminal compartment at the beginning of the assay while filling abluminal compartment with prewarmed high glucose DMEM. For the basal/control groups, cells were exposed to prewarmed high glucose DMEM in both the luminal and abluminal compartments. We chose high glucose DMEM as the diluent in the stimulant because we observed a non-linear digital sensor signal response in the spike-in KC calibration curves when using ECM (Fig. S3). The non-linearity is possibly due to the matrix effect and the interference of multiple growth factors that are added in the ECM.

2.4. DigiTACK longitudinal assay and readout

At the first time point of interest after the LPS stimulation, the DigiTACK devices were moved from the 37 °C incubator to a roomtemperature biosafety cabinet. The DigiTACK longitudinal assay started with moving the Component 1 strip to a location on the Component 2 wafer where each abluminal compartment fluid was paired with and exposed to a set of digital sensor patches (Fig. 2A). Here, pressure was applied to ensure the sealing between the PDMS layer of the Component 1 strip and the glass substrate of Component 2. Recording the cytokine concentrations in the abluminal compartment fluid requires the fluid to be in contact with the digital sensor patches only for 15 min, which we refer to as "pre-equilibrium digital fingerprinting." At the end of the preequilibrium digital fingerprinting process, the Component 1 strip was moved to another sensor-free location on the Component 2 wafer. At the subsequent time points, we repeated the assay procedure, which involved moving the strip to a location with a new set of digital sensor patches and pre-equilibrium digital fingerprinting (Fig. 2A, B,2C). This digital fingerprinting technique allows dilution-free low-concentration analyte detection without altering the abluminal microenvironment. In contrast, conventional ex situ measurement of these microfluidic volumes <20 μL would involve diluting the supernatant and replenishing the abluminal compartments with fresh culture medium at every time point, which leads to sensitivity loss and undesirable microenvironment concentration alterations. The Component 2 wafer currently incorporates 28 sets of digital sensor patches. Employing multiple Component 2 wafers can further expand the assay's capacity to accommodate a larger number of digital fingerprinting time points or conditions than tested in this study.

At the end of the longitudinal assay, the Component 1 strip was removed from the Component 2 wafer and attached to a thin microscope coverslip for downstream tissue fixation and immunofluorescent staining/imaging. The Component 2 wafer was subsequently attached to a PDMS assay layer (Fig. 2D) for downstream high-throughput digital immunosensor signal readout under room temperature in a dark optical room. The signal readout process involves detection-antibody labeling (MCP1 (#506002, BioLegend, USA), IL-6 (#504601 BioLegend, USA), KC (# DY453-05, Bio-Techne, USA)), horseradish

peroxidase (HRP) labeling, washing (5 min after detection antibody and HRP labeling in PBS + 0.05% Tween 20), substrate loading (QuantaRed™ Enhanced Chemifluorescent HRP Substrate, Thermo Fisher, USA), and sealing with fluorocarbon oil (Novec™ 7500, 3M, USA) to physically isolate and compartmentalize each microwell from others. The Component 2 wafer attached to the PDMS assay layer was then placed on the motorized stage of a fluorescent microscope. We pre-programmed the motorized stage such that it scanned every digital sensor patch on the Component 2 wafer. The batched offline sensor reading strategy in the assay downstream ensures high-throughput data acquisition.

During the digital immunosensor signal readout process, a QuantaRed fluorescent channel (545 nm/605 nm, excitation/emission) was used to count the "on" microwell spots at each sensor patch. The number of the "on" spots directly correlates to the target analyte's concentration (Fig. 2D). Scanning the entire images of the digital immunosensor microwells on the Component 2 wafer took less than 10 min. Standards for mouse MCP1, IL-6 and KC to generate DigiTACK calibration curves were all obtained from R&D system's DuoSet ELISA kits (MCP1: #DY479, IL-6: #DY40605, KC: # DY45305). We used ELISA to validate the DigiTACK measurements of MCP1, IL-6 and KC. The MCP1 and IL-6 ELISA measurements were performed by the standard plate coating and assay protocol using antibody pairs from BioLegend mentioned above. KC ELISA measurements were done with R&D systems Mouse KC DuoSet ELISA kits (# DY453-05, Bio-Techne, USA).

2.5. Data analysis by a convolutional neural network

We processed all scanned digital immunosensor images using our previously reported convolution neural network (CNN) algorithm. The algorithm runs two signal recognition pathways in parallel. One CNN recognizes and counts the enzyme active "On" microwells and the other recognizes defects and contaminations. The algorithm starts from a preprocessing process, including image cropping, contrast enhancement, noise filtering, light source uniformity and background correction. The CNN then classifies each image pixel into two categories: (1) image defects and (2) background. The "On" microwells counted by ImageJ are segmented out as the output mask with defects removed. More details in the machine learning algorithms can be found in our previously reported paper (Song et al., 2021b) Lastly, the fraction of the "On" microwells with respect to the total microwells (P_{on}) is calculated, and the Poisson's distribution equation $P(x = k) = \lambda k/k! \exp(-\lambda)$ is used to calculate λ. Here, k is the number of occurrences, and λ is the average number of events. P_{on} is the probability sum of P for k = 1, 2, 3, 4, …, ∞. Therefore, $P_{on} = 1 - P(x = 0)$ gives $\lambda = -\ln(1 - P_{on})$, which represents the average number of analytes per compartment (AAC) in digital assays and is proportional to the analyte concentration (Zhang and Noji, 2017).

2.6. Immunofluorescent staining

At the end of the DigiTACK longitudinal assay, the Component 1 strip was detached from the Component 2 wafer, and it was resealed on top of a microscope slide cover slip (Fisherbrand 24x60-1, Thermo Fisher, USA). The mBMECs cultured in the Component 1 strip were then fixed with 4% paraformaldehyde for 15 min at room temperature (RT), followed by three 5-min washes with phosphate-buffered saline (PBS). The luminal compartments were later incubated in blocking solution (0.05% TritonX-100, 5% normal

goat serum, 1X PBS) for 1 h at RT. Then, we added fluorescently labelled primary antibodies targeting ZO-1 and Claudin-5 (#352588, #339194, Thermo Fisher, USA) (dilution of 1:100 in blocking solution) to the sample and incubated at 4 °C overnight. The devices were washed with PBS and incubated with DAPI (1:500 dilution in PBS) for 2 h at RT. After the PBS washing process, the mBMEC tissues in the Component 1 strip became ready for fluorescent or confocal microscopy.

2.7. COMSOL finite element analysis

We assumed a constant cytokine flux into the bottom abluminal compartment fluid across the membrane during the secretion period. The flux value was back calculated from the endpoint measurements of the analytes. Using the flux value, the KC concentration distribution in the bottom abluminal compartment was simulated after 2 h of secretion, where the simulation accounted for the lateral diffusion of the analyte molecules entering the channel through the membrane pores. The simulation solved the convection-diffusion equation (Eq. (1)).

$$\frac{\partial c}{\partial t} = \nabla \bullet (D \nabla c) - \nabla \bullet (uc) + R \quad \text{(Eq. 1)}$$

where c is the analyte concentration, t is time, D is the analyte diffusion coefficient, u is the velocity of the abluminal compartment fluid in convection, and R is the analyte generation (annihilation) rate of the source (sink) in the system. Due to the small molecular weight of cytokines and the slight height dimensions of the microfluidic device, gravity-induced particle drifting has minimal effect on the vertical concentration distribution. Therefore, the concentration distribution during the secretion period is mainly governed by the analyte flux from the cells and the subsequent analyte diffusion. The value of D was obtained from the Stokes-Einstein equation (Eq. (2)), and the analyte's Stokes radius R was estimated by Eq. (3).

$$D = \frac{kT}{6\pi\eta R} \quad \text{(Eq. 2)}$$

$$R = \sqrt[3]{\frac{3MW}{4\pi N_A}\upsilon} \quad \text{(Eq. 3)}$$

Here, the k is the Boltzmann constant, T is the temperature, η is the viscosity of the abluminal compartment fluid, and R is the Stokes radius of the analyte molecule. To use Eq. (3), we assumed a spherical structure with closely packed atoms for the KC molecule. Here, MW is the molecular weight of KC, N_A is the Avogadro's number, and v is the partial specific volume of KC, which was estimated to be the typical value for proteins, 0.73 g/cm^3 (Erickson, 2009). These estimated values were used in our finite element analysis by COMSOL to predict the post-secretion KC concentration distribution (Fig. 3D(i), Video S1). Subsequently, we simulated the transient KC distribution under convective mixing of the abluminal compartment fluid. The convective mixing was generated by oscillating the directions of a laminar inflow through the abluminal compartment inlet/outlet ports under

no-slip boundary conditions (video S2). High mixing efficiency of the simulated process was experimentally validated as shown in Fig. S4.

Supplementary video related to this article can be found at https://doi.org/10.1016/j.bios.2022.115030.

2.8. Statistics

All error bars in the graphs shown represent a standard deviation unless otherwise specified. Group analysis was all performed using an unpaired Welch's *t*-test, and a p-value of <0.05 was considered as statistically significant. The digital immunosensor assay standard curves were fitted with a 4-parameter logistic regression by GraphPad Prism 9 (GraphPad Software, USA). The LoD of every marker was determined by the signal corresponding to three times the standard deviation above the average blank signal.

3. Results and discussion

3.1. DigiTACK assay with multiplexed beadless digital counting sensors

DigiTACK is a reversibly sealable Barrier-on-a-Chip microfluidic device that includes two components. The top part (Component 1) consists of two fluidic compartments (luminal and abluminal) separated by a brain endothelial cell (mBMEC) barrier grown on top of a NPN membrane (Fig. 1B(i)). The bottom part (structural unit of Component 2) is a beadless digital counting glass chip fabricated by conventional lithography patterning, etching, and novel exfoliation-based antibody patterning to achieve high-density antibody immobilization within microwells (Fig. S1). An array of three rectangular patterns (89,760 microwells) forms one of the digital sensor patches for profiling one abluminal compartment in Component 1 (Fig. 1B(i), 1B(iv), 1B(v)). The large number of microwells per digital sensor patch allows for reducing the assay coefficient of variance (CV) that originates from Poisson noise (Rissin et al., 2010).

We pair each digital sensor patch patterned on a location of the Component 2 glass wafer with one of the abluminal compartments in the Component 1 strip. Each digital sensor patch location is specifically assigned to detect the concentration profiles of three different protein analytes in the abluminal compartment fluid at a different assay time point or under different assay conditions (Fig. 2). The arrayed DigiTACK configuration enables high-throughput profiling of mBMEC tissue-secreted cytokines. The DigiTACK longitudinal measurement in this study involves moving the Component 1 strip from one location to another on the Component 2 wafer (Fig. 2A, B, 2C). Upon the completion of the longitudinal measurement, the digital senor patches on the Component 2 wafer retain all the analyte concentration information obtained at different time points. This information is read out from the parallelly labelled digital sensors on the Component 2 wafer via singlemolecule digital counting (Fig. 2D).

3.2. Characterization of DigiTACK performance

Using high glucose DMEM spiked by known concentrations of MCP1, IL-6 and KC, we obtained standard curves for these three analytes and determined their LoD values of

0.576, 0.101, 0.433 pg/mL, respectively (Fig. 3A). The whole standard curve acquisition process for the three analytes required only 15 min. From preliminary experiments with LPS stimulated endothelial cells, we observed that after 10 h of secretion, MCP1 and KC concentrations reached up to ~6000 and 20000 pg/mL levels, respectively. Therefore, we decreased the concentrations of the MCP1 and KC sensor's detection antibody and the HRP label to maintain signal linearity at high concentrations for prolonged stimulation experiments. Overall, we obtained ultrahigh sensitivity and a linear dynamic range of ~4 orders of magnitude (~0.1 pg/mL to ~1000 pg/mL) for the DigiTACK immunosensors, and we could extend the linear dynamic range by 1–2 orders of magnitude with lowered labeling efficiency. Additionally, the beadles assay format used in the assay could further improve the sensor's linear dynamic range. Directly immobilizing capture antibodies within microwell bottoms, this method eliminates the stochastic process of beads settling into microwells by gravity, which is typically employed in the conventional bead-based digital immunoassay yielding a ~55% microwell filling rate (Song et al., 2021b). As a result, our method can achieve 100% utilization of the microwell sites for the assay, thus suppressing sensor signal saturation and Poisson noise and offering a larger digital linear dynamic range and smaller CV for a given sensor area size. Notably, we did not observe any cross-reactivity between the three markers utilizing this beadless format (Fig. S5).

In the DigiTACK measurement, the digital immunosensors uptake only a miniscule portion of the analytes from the assayed bulk solution. We first define the "analyte utilization rate" as the fraction of the number of the analyte molecules taken for the measurement to the total number of the molecules present in the original sample fluid. The Poisson statistics-derived average-analyte-per-compartment (λ) times the total number of compartments in the sensors represents the total number of the molecules captured by a single digital sensor patch. We further divide the total captured molecules by the total number of molecules in the assayed sample volume, providing an average utilization rate (Fig. 3B). The utilization rate from 0.3 pg/mL to 1000 pg/mL are all well below 0.1% for all three markers. Thus, the sensors do not alter the analyte concentration of the bulk sample fluid even when operating at low concentration levels. The gradual increase of the utilization rate with the decreasing concentration is due to the sensor signals approaching the nonspecific binding of HRP background, not due to a greater proportion of analyte uptake (Fig. 3B). We measured the same cell secreted markers using both the gold standard ELISA and the 3-plex DigiTACK assay. We found excellent correlation between the two assay methods ($R^2 = 0.9778$) (Fig 3C). From the linear fitting formula, the slope is 0.8888, which indicates the high accuracy of the 3-plex DigiTACK assay compared to the gold standard single-plex ELISA.

The experiment is performed under the condition where the tissue-secreted analytes are measured within a microfluidic device experiencing little bulk fluid flow or mixing during the tissue culture experiment. We then examined how analyte exposure to the digital sensor patches would reflect the total analyte content in the abluminal compartment fluid under such a condition. Finite element analysis was performed on the abluminal compartment fluid as indicated in Fig. 3D(i). The result shows that the concentration is highly non uniform, and mixing is needed for accurate and reproducible multiplexed measurements by the spatially encoded digital sensors. We therefore further modeled the concentration profile after oscillatory mixing events using multiple laminal inflows through the ports (Fig.

3D(ii), Video S2). We observed that the geometry of the bottom abluminal compartment can create sufficient homogenizing effects through the oscillating flows. With only 4 oscillation cycles, the concentrations on top of the sensor areas become nearly the same as each other. We plotted the standard deviation of the averaged surface concentration on three sensor cut planes (shown in the inset of Fig. 3E) throughout the mixing period and quantitatively characterized the mixing efficiency (Fig. 3E). The standard deviation decreases and approaches 0 after just a few cycles. For consistency, we applied 20 cycles of oscillation mixing to all devices at every measurement time point using a programmed 8-channel peristaltic pump (Experimental verification of mixing efficiency shown in Fig. S4).

Supplementary data related to this article can be found at https://doi.org/10.1016/j.bios.2022.115030.

3.3. Imaging of primary mouse brain microvascular endothelial cell barriers cultured in DigiTACK

Primary mouse brain microvascular endothelial cells (mBMECs) were cultured to confluence and formed tight junctions on the NPN membrane in the DigiTACK device (Fig. 4A(I), 4A(III)). We did not observe significant morphological differences before and after the DigiTACK longitudinal assay, which involves the repeated relocation and bonding/debonding of the Component 1 strip on the Component 2 wafer (Fig. 4A(II), 4A(IV)). This can be attributed to the ability of the NPN membrane to hydraulically decouple the top luminal and bottom abluminal compartments. Across the membrane, diffusion is seamless while incidental convection is stopped by the high flow resistance of the 60 nm pores. Therefore, cells on the membrane are protected despite being <100 nm away from the fluidic disturbances in the abluminal compartment (Chung et al., 2014). Furthermore, we performed immunofluorescent staining on tight junction proteins ZO-1 (Alexa Fluor 594) and Claudin-5 (Alexa Fluor 488). In all samples, continuous ZO-1 and Claudin 5 staining was detected at the borders of the mBMECs, indicating the presence of an intact and functional barrier. We observed slight morphological changes in junctional protein Claudin-5 and ZO-1 in LPS-treated groups, which were manifested as defragmented staining (Fig. 4B(I) vs. 4B(II)). The DigiTACK assay remains compatible with real-time brightfield imaging and end point immunofluorescent staining, which are commonly performed for quality control in tissue chip workflows. The qualitative nature of the immunofluorescent staining provides some level of understanding of the cultured tissue's functions. But it does not capture any quantitative signature differences in the cell phenotype under these stimulation conditions, which again highlights the need for an integrated immunosensor in BBB-oC platforms.

3.4. Longitudinal multiplexed protein secretion monitoring of endothelial barriers

Using the DigiTACK platform, we measured the temporal concentration changes of the 3 mBMEC tissue barrier-secreted cytokine markers at three time points during 10 h of cell stimulation/culture (2-h, 6-h, and 10-h) (Fig. 5). At each time point, we measured the cytokine concentrations in the abluminal compartment fluid in situ by a 15-min pre-equilibrium digital fingerprinting process with the integrated immunosensors (see Materials

and Methods). The large sample volume >100 μL held in the top luminal compartment in Component 1 allowed sequential collection of a 10 μL supernatant. We collected a set of luminal compartment fluid supernatants from the Component 1 strip in parallel using a multichannel micropipette without altering the original luminal cytokine concentrations, loaded the supernatants onto the luminal sample measurement device (Fig. S2C), and measured the luminal cytokine concentrations for these samples in a single batch of experiment.

From the luminal-side data in Fig. 5A, B and 5C, we observed a significant cytokine secretion response following the 500 ng/mL LPS stimulation. All three markers plateaued at around the 10-h time point with MCP1 and KC approaching ~6000 pg/mL and ~20000 pg/mL, respectively. The IL-6 level stabilized at ~100 pg/mL for the stimulated groups. All basal condition samples showed low cytokine secretion levels throughout the longitudinal experiment. Interestingly, we were able to capture significant differences between the stimulated and basal groups even at 2 h for MCP1 ($p = 0.002$) and KC ($p = 0.04$). Although IL-6 also started rising as soon as 2 h after stimulation, the variability in secretion was much greater. At 2 h, all 3 markers were significantly elevated by LPS stimulation.

From the abluminal-side data in Fig. 5D, E and 5F, we found that the cytokine secretion level was lower and also more variable than in the luminal compartment. In the basal condition, the abluminal cytokine secretion level remained low during 10 h of culture. MCP1 and IL-6 concentrations were both above the basal conditions at 6 h after stimulation, although the high data variability precluded statistically significant differences from controls ($p = 0.06$ and 0.1 respectively). The abluminal KC profile, however, showed a linear trend throughout the 10-h LPS stimulation period and even showed significant differences between the stimulation and basal conditions at the 2-h time point ($p = 0.02$, stimulated average 219.2 pg/mL vs. basal average 90.8 pg/mL). At the 10-h time point, the KC concentration for the stimulation condition reached an average value of 6920.3 pg/mL, and its trend showed no sign of saturation.

The data show significantly polarized cytokine secretion behavior for the same marker between the luminal and abluminal sides of the endothelial barrier. At 10 h, we see concentration gradients across the barrier in favor of luminal secretion as large as ~5000 pg/mL (~25-fold differences) for the MCP1, and ~13700 pg/mL for KC (~3-fold differences). The stimulation on one side of the barrier may have induced some level of the polarization of the brain endothelial cells, resulting in more secretion events at the stimulated luminal side than the abluminal side.

4. Conclusion and outlook

Capturing cytokine secretion profiles in BBB-oC systems is critical in assessing CNS therapeutic side effects and understanding disease mechanisms relating to neuroinflammation caused by the infiltration of bloodborne cells or substrates (e.g., multiple sclerosis, encephalitis, strokes). The literature has reported cytokines' roles in neurological disorders either as factors that induce leukocyte infiltration, or as factors that more directly cause neural tissue damage. However, in-depth understanding of these disease progressions

remains unknown either due to the difficulty of separating variables in complex in vivo models or the current insufficient and granular data restricted by end-point measurements with previous BBB-oC platforms.

To address the challenges above, we have developed the *first* Barrier-on-a-Chip platform to feature integrated immunosensors named “DigiTACK.” Permitting a novel beadless microwell digital assay within the Barrier-on-a-chip, DigiTACK offers ultrasensitive multiplexed abluminal cytokine concentration measurements with LoDs of a few hundreds of fg/mL while minimizing the assay time and maintaining an excellent correlation with the gold standard ELISA measurements. Additionally, the DigiTACK assay simultaneously allows for real-time brightfield imaging and end-point immunofluorescent staining characterization of the brain barrier. We designed the reversible “tacking and fingerprinting” strategy for the abluminal cytokine measurements to address several difficulties and requirements associated with immunosensing in the microfluidic Barrier-on-a-Chip platform. First, the small sample volume (<20 μL) of the abluminal compartment on each tissue culturing device prohibits supernatant extraction from the sample. If the measurement was carried out ex situ, the assay would require diluting the supernatant and replenishing the culture medium, which result in sensitivity loss and microenvironment alterations. In contrast, implementing the digital fingerprinting technique here allows dilution-free low-concentration analyte detection without altering the abluminal microenvironment. Second, a previous study (Naegelen et al., 2015) indicates that analyte concentrations in a cell-containing environment can decrease during a longitudinal experiment due to the cellular intake or degradation of analytes. Resetting or renewing the sensors at each measurement time point is necessary to capture these concentration fluctuations. The reversible “tacking and fingerprinting” assay strategy of this study achieves this by moving and exposing an array of tissue culture devices to a new set of digital immunosensors at each time point.

In this study, we used a simplified LPS-stimulated mBMEC barrier model in the DigiTACK platform. Even the simple model allowed us to observe several interesting phenomena, such as (i) various concentration dynamic ranges and secretion rates for different cytokine markers, (ii) distinct cytokine responsiveness and homeostasis time points between the different sides of the barrier (i.e., secretion polarization), and (iii) marker-dependent gradient magnitudes across the mBMEC barrier. We observed that the secretion level approached steady state at about 6 h on the luminal side. In contrast, the concentrations of all three markers continued to climb on the abluminal side. This suggests that the abluminal cytokine secretion may experience a relatively delayed effect while the luminal secretion manifests a fast and drastic response. The linearly increasing KC levels on the abluminal side may eventually approach the luminal compartment concentration. We speculate that the KC concentration parity between the two sides may compel neutrophils to migrate across the endothelial barrier (Salminen et al., 2020). To prove this, more experiments with even longer stimulation are needed to see if the abluminal side eventually reaches steady state and determine at what concentration levels it occurs.

This paper presents the *first* study to provide sequential temporal in situ profiling of multiple cytokines/chemokines secreted from barrier tissues. The study indicates that the DigiTACK platform may find wide use in recording abrupt cytokine secretion changes

in response to a stimulus or cells introduced in sequentially controlled experiments. For example, for multiple sclerosis or stroke studies, the DigiTACK assay could facilitate parallel monitoring of cytokine concentration fluctuations upon observing or introducing immune cell infiltrations (Lopes Pinheiro et al., 2016). For dynamic BBB and CNS studies, by sequentially altering luminal fluids and removing stimulants, we could use the DigiTACK assay to capture the timing when the abluminal side of the BBB returns to its homeostatic cytokine concentration (DiSabato et al., 2016; Gilroy and Lawrence, 2008). The low molecular utilization rate and short pre-equilibrium profiling time of the integrated digital immunosensors proves the ultrahigh sensitivity and minimal invasiveness of the DigiTACK assay. Using these remarkable assay features, we could probe rapid non-classical cytokine secretory pathways that have been impossible to study with conventional methods. Such secretory pathways can be studied by measuring preformed cytokines' immediate release from granules (e.g., neutrophils) into the local microenvironment within minutes of receptor stimulation (Lacy and Stow, 2011).

The DigiTACK platform exhibits promising potential in sequential multiplexed cytokine profiling in an organ-on-a-chip. While this study was specifically aimed at validating DigiTACK's ability to characterize the secretory behavior of a mBMEC barrier for future BBB studies, the device can be applied with improved functions to any barrier-related organ-on-a-chip systems by switching the cultured cell types. Additionally, we are actively exploring other integrated modules to complement the DigiTACK device, including a flow module integrated into the top luminal reservoir for dynamic circulation and shear force modeling (Mansouri et al., 2022) and electrodes integrated into Component 1 for TEER measurements along with the DigiTACK immunosensing. Coupling these features with future human iPSC-derived pericytes, astrocytes and microglia co-cultured in the bottom abluminal compartment would form a more bio resembling, versatile BBB-on-a-chip platform. The platform can facilitate multiple studies of human CNS disease progression, and ultimately leading to OoC-guided, personalized precision medicine therapeutics.

Supplementary Material

Refer to Web version on PubMed Central for supplementary material.

Acknowledgements

M.C.M., J.L.M., S-H.S., M.S. B.H.S, and K.K. were partially supported by NIH R61HL154249. B.H.S. was partially supported by K08NS101054 and R01AG074968. S-H.S. and K.K. were partially supported by NSF CBET 1931905.

Data availability

Data will be made available on request.

References

Ahn SI, Sei YJ, Park HJ, Kim J, Ryu Y, Choi JJ, Sung HJ, MacDonald TJ, Levey AI, Kim Y, 2020. Microengineered human blood-brain barrier platform for understanding nanoparticle transport mechanisms. Nat. Commun 11 (1), 175. [PubMed: 31924752]

Badiola-Mateos M, Di Giuseppe D, Paoli R, Lopez-Martinez MJ, Mencattini A, Samitier J, Martinelli E, 2021. A novel multi-frequency trans-endothelial electrical resistance (MTEER) sensor array to monitor blood-brain barrier integrity. Sensor. Actuator. B Chem 334.

Carbone L, 2021. Estimating mouse and rat use in American laboratories by extrapolation from Animal Welfare Act-regulated species. Sci. Rep 11 (1), 493. [PubMed: 33436799]

Castro Dias M, Odriozola Quesada A, Soldati S, Bosch F, Gruber I, Hildbrand T, Sonmez D, Khire T, Witz G, McGrath JL, Piontek J, Kondoh M, Deutsch U, Zuber B, Engelhardt B, 2021. Brain endothelial tricellular junctions as novel sites for T cell diapedesis across the blood-brain barrier. J. Cell Sci 134 (8).

Chung HH, Chan CK, Khire TS, Marsh GA, Clark A Jr., Waugh RE, McGrath JL, 2014. Highly permeable silicon membranes for shear free chemotaxis and rapid cell labeling. Lab Chip 14 (14), 2456–2468. [PubMed: 24850320]

DiSabato DJ, Quan N, Godbout JP, 2016. Neuroinflammation: the devil is in the details. J. Neurochem 139 (Suppl. 2), 136–153. [PubMed: 26990767]

Erickson HP, 2009. Size and shape of protein molecules at the nanometer level determined by sedimentation, gel filtration, and electron microscopy. Biol. Proced. Online 11, 32–51. [PubMed: 19495910]

Gilroy D, Lawrence T, 2008. The resolution of acute inflammation: a ‘tipping point’ in the development of chronic inflammatory diseases. In: Rossi AG, Sawatzky DA (Eds.), The Resolution of Inflammation. Birkhäuser Basel, Basel, pp. 1–18.

Hudecz D, Khire T, Chung HL, Adumeau L, Glavin D, Luke E, Nielsen MS, Dawson KA, McGrath JL, Yan Y, 2020. Ultrathin silicon membranes for in situ optical analysis of nanoparticle translocation across a human blood-brain barrier model. ACS Nano 14 (1), 1111–1122. [PubMed: 31914314]

Lacy P, Stow JL, 2011. Cytokine release from innate immune cells: association with diverse membrane trafficking pathways. Blood 118 (1), 9–18. [PubMed: 21562044]

Larochelle C, Alvarez JI, Prat A, 2011. How do immune cells overcome the blood-brain barrier in multiple sclerosis? FEBS Lett. 585 (23), 3770–3780. [PubMed: 21550344]

Lecuyer MA, Kebir H, Prat A, 2016. Glial influences on BBB functions and molecular players in immune cell trafficking. Biochim. Biophys. Acta 1862 (3), 472–482. [PubMed: 26454208]

Liang Y, Yoon J-Y, 2021. In situ sensors for blood-brain barrier (BBB) on a chip. Sensors and Actuators Reports 3, 100031.

Lombardi A, Cantini G, Mello T, Francalanci M, Gelmini S, Cosmi L, Santarlasci V, Degl’Innocenti S, Luciani P, Deledda C, Annunziato F, Forti G, Galli A, Serio M, Luconi M, 2009. Molecular mechanisms underlying the pro-inflammatory synergistic effect of tumor necrosis factor alpha and interferon gamma in human microvascular endothelium. Eur. J. Cell Biol 88 (12), 731–742. [PubMed: 19782427]

Lopes Pinheiro MA, Kooij G, Mizee MR, Kamermans A, Enzmann G, Lyck R, Schwaninger M, Engelhardt B, de Vries HE, 2016. Immune cell trafficking across the barriers of the central nervous system in multiple sclerosis and stroke. Biochim. Biophys. Acta 1862 (3), 461–471. [PubMed: 26527183]

Low LA, Mummery C, Berridge BR, Austin CP, Tagle DA, 2021. Organs-on-chips: into the next decade. Nat. Rev. Drug Discov 20 (5), 345–361. [PubMed: 32913334]

Lv S, Song HL, Zhou Y, Li LX, Cui W, Wang W, Liu P, 2010. Tumour necrosis factor-alpha affects blood-brain barrier permeability and tight junction-associated occludin in acute liver failure. Liver Int. 30 (8), 1198–1210. [PubMed: 20492508]

Mansouri M, Ahmed A, Ahmad SD, McCloskey MC, Joshi IM, Gaborski TR, Waugh RE, McGrath JL, Day SW, Abhyankar VV, 2022. The modular microSiM reconfigured: integration of microfluidic capabilities to study in vitro barrier tissue models under flow. Adv Healthc Mater, e2200802. [PubMed: 35953453]

McCloskey MC, Kasap P, Ahmad SD, Su SH, Chen K, Mansouri M, Ramesh N, Nishihara H, Belyaev Y, Abhyankar VV, Begolo S, Singer BH, Webb KF, Kurabayashi K, Flax J, Waugh RE, Engelhardt B, McGrath JL, 2022. The modular microSiM: a mass produced, rapidly assembled,

and reconfigurable platform for the study of barrier tissue models in vitro. Adv Healthc Mater 11 (18), e2200804. [PubMed: 35899801]

Mir M, Palma-Florez S, Lagunas A, Lopez-Martinez MJ, Samitier J, 2022. Biosensors integration in blood-brain barrier-on-a-chip: emerging platform for monitoring neurodegenerative diseases. ACS Sens. 7 (5), 1237–1247. [PubMed: 35559649]

Mossu A, Rosito M, Khire T, Li Chung H, Nishihara H, Gruber I, Luke E, Dehouck L, Sallusto F, Gosselet F, McGrath JL, Engelhardt B, 2019. A silicon nanomembrane platform for the visualization of immune cell trafficking across the human blood-brain barrier under flow. J. Cerebr. Blood Flow Metabol 39 (3), 395–410.

Naegelen I, Beaume N, Plancon S, Schenten V, Tschirhart EJ, Brechard S, 2015. Regulation of neutrophil degranulation and cytokine secretion: a novel model approach based on linear fitting. J. Immunol. Res, 817038, 2015.

Obermeier B, Daneman R, Ransohoff RM, 2013. Development, maintenance and disruption of the blood-brain barrier. Nat. Med 19 (12), 1584–1596. [PubMed: 24309662]

Oddo A, Peng B, Tong Z, Wei Y, Tong WY, Thissen H, Voelcker NH, 2019. Advances in microfluidic blood-brain barrier (BBB) models. Trends Biotechnol. 37 (12), 1295–1314. [PubMed: 31130308]

Ortega MA, Fernandez-Garibay X, Castano AG, De Chiara F, Hernandez-Albors A, Balaguer-Trias J, Ramon-Azcon J, 2019. Muscle-on-a-chip with an on-site multiplexed biosensing system for in situ monitoring of secreted IL-6 and TNF-alpha. Lab Chip 19 (15), 2568–2580. [PubMed: 31243422]

Rissin DM, Kan CW, Campbell TG, Howes SC, Fournier DR, Song L, Piech T, Patel PP, Chang L, Rivnak AJ, Ferrell EP, Randall JD, Provuncher GK, Walt DR, Duffy DC, 2010. Single-molecule enzyme-linked immunosorbent assay detects serum proteins at subfemtomolar concentrations. Nat. Biotechnol 28 (6), 595–599. [PubMed: 20495550]

Salminen AT, Tithof J, Izhiman Y, Masters EA, McCloskey MC, Gaborski TR, Kelley DH, Pietropaoli AP, Waugh RE, McGrath JL, 2020. Endothelial cell apicobasal polarity coordinates distinct responses to luminally versus abluminally delivered TNF-alpha in a microvascular mimetic. Integr. Biol 12 (11), 275–289.

Schilling M, Strecker JK, Ringelstein EB, Kiefer R, Schabitz WR, 2009. Turn-over of meningeal and perivascular macrophages in the brain of MCP-1-, CCR-2- or double knockout mice. Exp. Neurol 219 (2), 583–585. [PubMed: 19615366]

Song Y, Sandford E, Tian Y, Yin Q, Kozminski AG, Su SH, Cai T, Ye Y, Chung MT, Lindstrom R, Goicochea A, Barabas J, Olesnavich M, Rozwadowski M, Li Y, Alam HB, Singer BH, Ghosh M, Choi SW, Tewari M, Kurabayashi K, 2020. Rapid single-molecule digital detection of protein biomarkers for continuous monitoring of systemic immune disorders. Blood 137 (12), 1591–1602.

Song Y, Ye Y, Su S-H, Stephens A, Cai T, Chung M-T, Han MK, Newstead MW, Yessayan L, Frame D, Humes HD, Singer BH, Kurabayashi K, 2021a. A digital protein microarray for COVID-19 cytokine storm monitoring. Lab Chip 21 (2), 331–343. [PubMed: 33211045]

Song Y, Zhao J, Cai T, Stephens A, Su S-H, Sandford E, Flora C, Singer BH, Ghosh M, Choi SW, Tewari M, Kurabayashi K, 2021b. Machine learning-based cytokine microarray digital immunoassay analysis. Biosens. Bioelectron 180, 113088. [PubMed: 33647790]

Stowe AM, Wacker BK, Cravens PD, Perfater JL, Li MK, Hu RL, Freie AB, Stuve O, Gidday JM, 2012. CCL2 upregulation triggers hypoxic preconditioning-induced protection from stroke. J. Neuroinflammation 9 (1), 1–12. [PubMed: 22212381]

Su SH, Song Y, Newstead MW, Cai T, Wu M, Stephens A, Singer BH, Kurabayashi K, 2021. Ultrasensitive multiparameter phenotyping of rare cells using an integrated digital-molecular-counting microfluidic well plate. Small 17 (31), e2101743. [PubMed: 34170616]

Williams JL, Holman DW, Klein RS, 2014. Chemokines in the balance: maintenance of homeostasis and protection at CNS barriers. Front. Cell. Neurosci 8, 154. [PubMed: 24920943]

Wolff A, Antfolk M, Brodin B, Tenje M, 2015. In vitro blood-brain barrier models-an overview of established models and new microfluidic approaches. J. Pharmacol. Sci 104 (9), 2727–2746.

Yu F, Kumar NDS, Foo LC, Ng SH, Hunziker W, Choudhury D, 2020. A pump-free tricellular blood-brain barrier on-a-chip model to understand barrier property and evaluate drug response. Biotechnol. Bioeng 117 (4), 1127–1136. [PubMed: 31885078]

Zhang Y, Noji H, 2017. Digital bioassays: theory, applications, and perspectives (vol 89, pg 92, 2017). Anal. Chem 89 (24), 13675–13675. [PubMed: 29192762]

Zhang YS, Aleman J, Shin SR, Kilic T, Kim D, Mousavi Shaegh SA, Massa S, Riahi R, Chae S, Hu N, Avci H, Zhang W, Silvestri A, Sanati Nezhad A, Manbohi A, De Ferrari F, Polini A, Calzone G, Shaikh N, Alerasool P, Budina E, Kang J, Bhise N, Ribas J, Pourmand A, Skardal A, Shupe T, Bishop CE, Dokmeci MR, Atala A, Khademhosseini A, 2017. Multisensor-integrated organs-on-chips platform for automated and continual in situ monitoring of organoid behaviors. Proc. Natl. Acad. Sci. U. S. A 114 (12), E2293–E2302. [PubMed: 28265064]

Zhu J, He J, Verano M, Brimmo AT, Glia A, Qasaimeh MA, Chen P, Aleman JO, Chen W, 2018. An integrated adipose-tissue-on-chip nanoplasmonic biosensing platform for investigating obesity-associated inflammation. Lab Chip 18 (23), 3550–3560. [PubMed: 30302487]

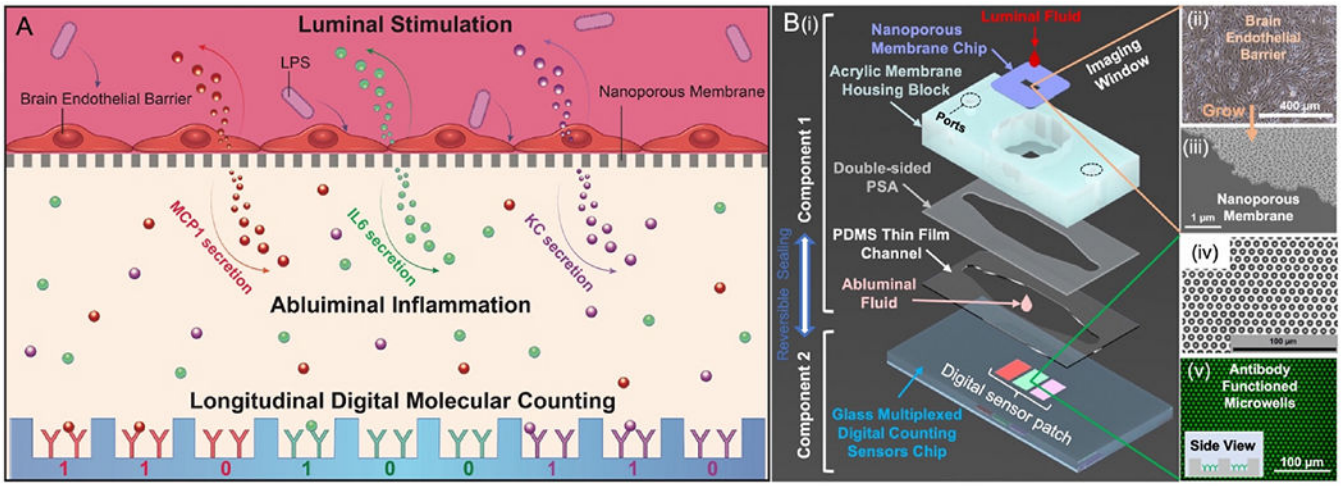

Fig. 1.

(A) Conceptual schematic of the integrated DigiTACK measurement of abluminal (brain)-side cytokine concentration via spatially-encoded-antibody-functioned microwells. Upon LPS stimulation, the brain microvascular endothelial cells secrete significant amounts of MCP1, IL-6 and KC to both sides of the barrier, which could cause systemic neuroinflammation. The captured analytes are later digitally counted for concentration quantification. (B) (i) Exploded view of one DigiTACK device which contains two components that are reversibly sealed. Component 1: A nanoporous silicon nitride (NPN) membrane chip is mounted onto a recessed acrylic membrane housing block. The bottom surface of the housing block is irreversibly bonded to a PDMS thin film cutout channel using a double-sided PSA. Together, Component 1 creates a Transwell-style open well reservoir for luminal (blood) fluid/stimulation in the top compartment and a bottom abluminal microfluidic channel compartment. The two compartments are connected only through the suspended NPN/cell membrane interface. Component 2: A glass wafer with arrayed digital sensor patches fabricated through DGRIE and micropatterning. Each digital sensor patch contains 3 rectangular arrays (89,760 microwells/array) that fits under the PDMS abluminal compartment with each array targeting a different analyte. The soft bottom PDMS thin film channel layer of Component 1 acts like an O-ring that allows reversible sealing to the Component 2 wafer. (ii) Phase contrast image of brain microvascular endothelial cells cultured in the device. (iii) SEM image of a NPN membrane. The membrane has a ~15% porosity (60 nm pores) and a ~50 nm thickness. (iv) Brightfield image of the DGRIE-etched glass microwells. Microwells are 3.8 μm in diameter and 3.5 μm in depth. (v) Fluorescent image of antibody specifically functioned within the microwells. Alexa fluor 488 anti-rat-IgG antibodies were used to label and visualize the distribution of mouse IL-6 capture antibodies.

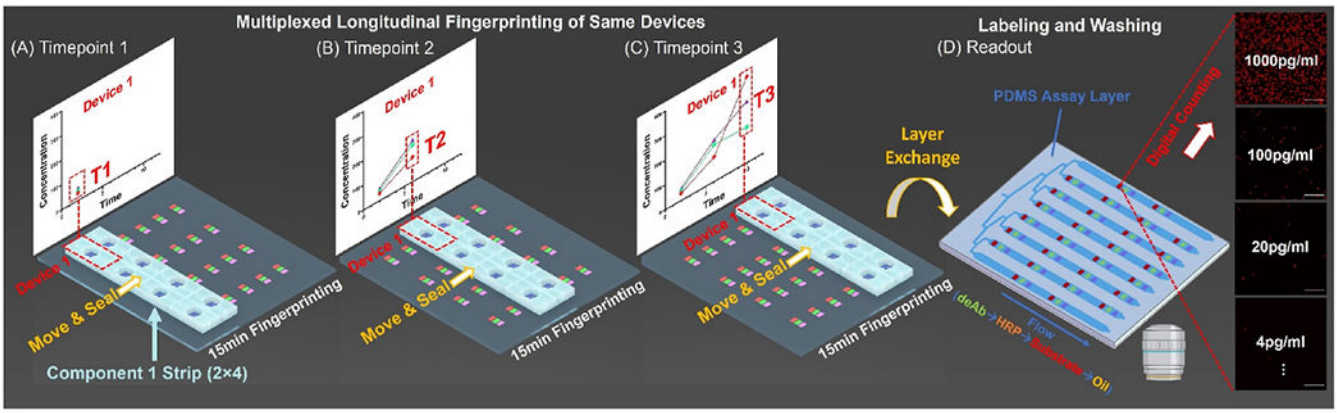

Fig. 2.

(A–D) Assay procedure of multiplexed longitudinal digital fingerprinting. (A) At the first time point of interest (T1), a Component 1 strip holding abluminal fluid samples assayed for different stimulation conditions or replicates in 2 × 4 DigiTACK devices is moved and reversibly sealed to a set of digital sensor patches on the Component 2 wafer. The exposed patches are in contact with the abluminal fluids for 15 min. The set of sensor patches at the location designated at T1 captures the three abluminal analytes and records their concentrations for the 8 devices. (B) At T2, the Component 1 strip and the bottom fluid is moved and resealed to the next location on the Component 2 wafer. The new set of digital sensor patches on the Component 2 wafer again records the 3-plexed concentration information at T2 across all 8 devices. (C) Similar to (B), the Component 1 strip is moved to the third location with another set of digital sensor patches, and the same multiplexed information is retained for T3. Supernatants of 10 μL from the top luminal reservoirs of the 8 DigiTACK devices were also sampled and frozen at each time point for a downstream massive parallel measurement. (D) The Component 1 strip is replaced with a PDMS layer with assay reagent channels (“PDMS assay layer”) on top of the Component 2 wafer to perform high-throughput detection-antibody labeling, HRP labeling, washing, substrate loading and oil sealing for every digital sensor patch. The Component 2 wafer is then scanned on a fluorescent microscope for digital molecular counting at each sensor patch. Representative digital counting images at different concentrations are shown on the right. The unlabeled scale bar is 100 μm.

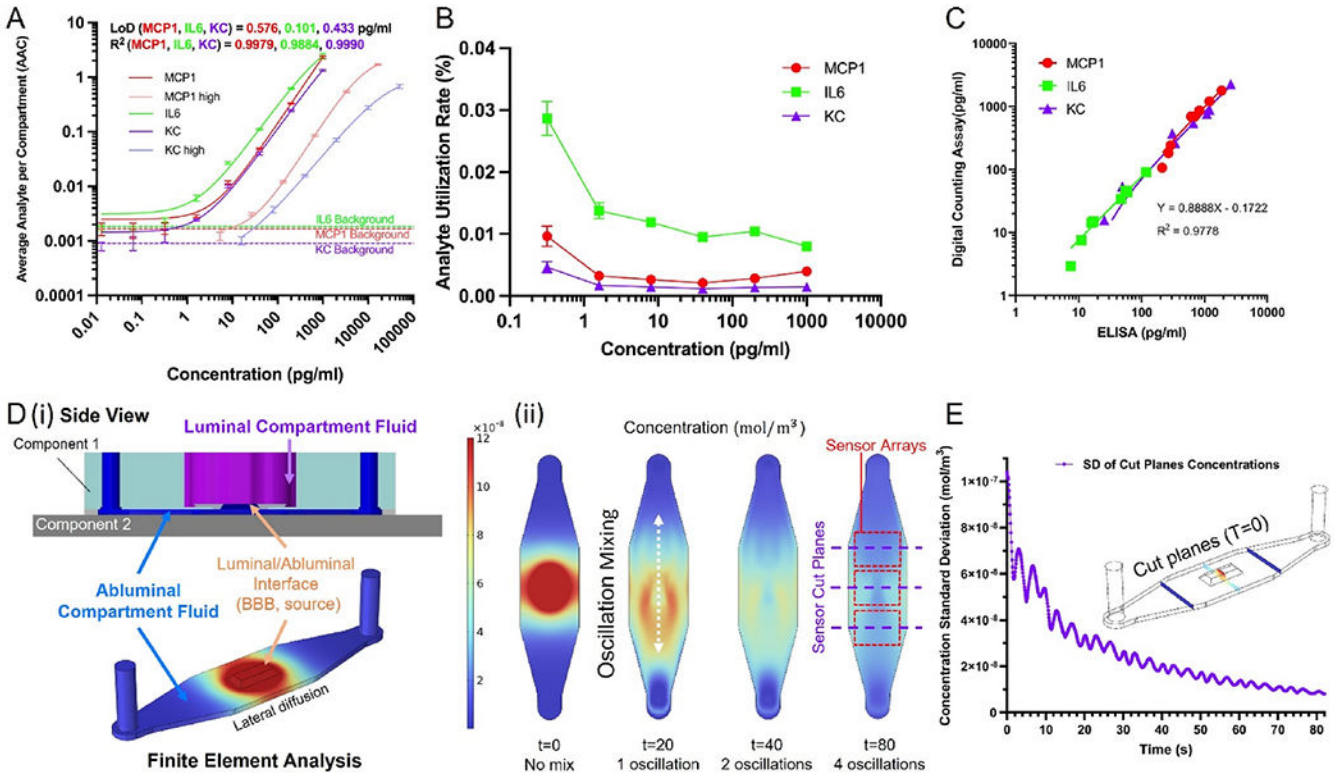

Fig. 3.

(A) Calibration curves of 3-plex DigiTACK assay. The limit of detection (LoD) values are obtained from the average blank signals plus 3 standard deviations. The LoDs of MCP1, IL-6 and KC are 0.576, 0.101, and 0.433 pg/mL respectively. Extra plots are generated for the large-dynamic-range calibration curves of MCP1 and KC since extremely high levels of these two markers are observed after prolonged stimulation. (>10 h) The increased linear dynamic range is achieved by reducing the labeling reagent concentration during the “Labeling and Washing” step in Fig. 2D. (B) Analyte utilization rate plotted against the concentration of the assayed sample solution. The utilization rate is defined as the fraction of the number of molecules captured by the sensor region to the total number of molecules present in the original bulk sample solution. Single molecule counting sensors take up a minuscule amount of analytes from the bulk solution, which is crucial to low-abundance analyte measurement without altering the sample microenvironment. (C) Excellent measurement correlation (R^2 = 0.9778) between the gold standard ELISA and the 3-plex DigiTACK assay. (D)(i) Finite element analysis shows a non-uniform concentration distribution across different regions in the bottom abluminal compartment after 2-hr of analyte secretion and lateral diffusion. (ii) Finite element analysis demonstrates that an oscillating laminar flow homogenizes the abluminal compartment fluid. The concentration distribution becomes fairly uniform only after 4 oscillation cycles. (E) Concentration standard deviation of the 3 cut planes (shown in inset) versus the mixing duration. The standard deviation of the analyte concentration decreases as the mixing operation proceeds, quantitatively showing the effectiveness of the mixing operation.

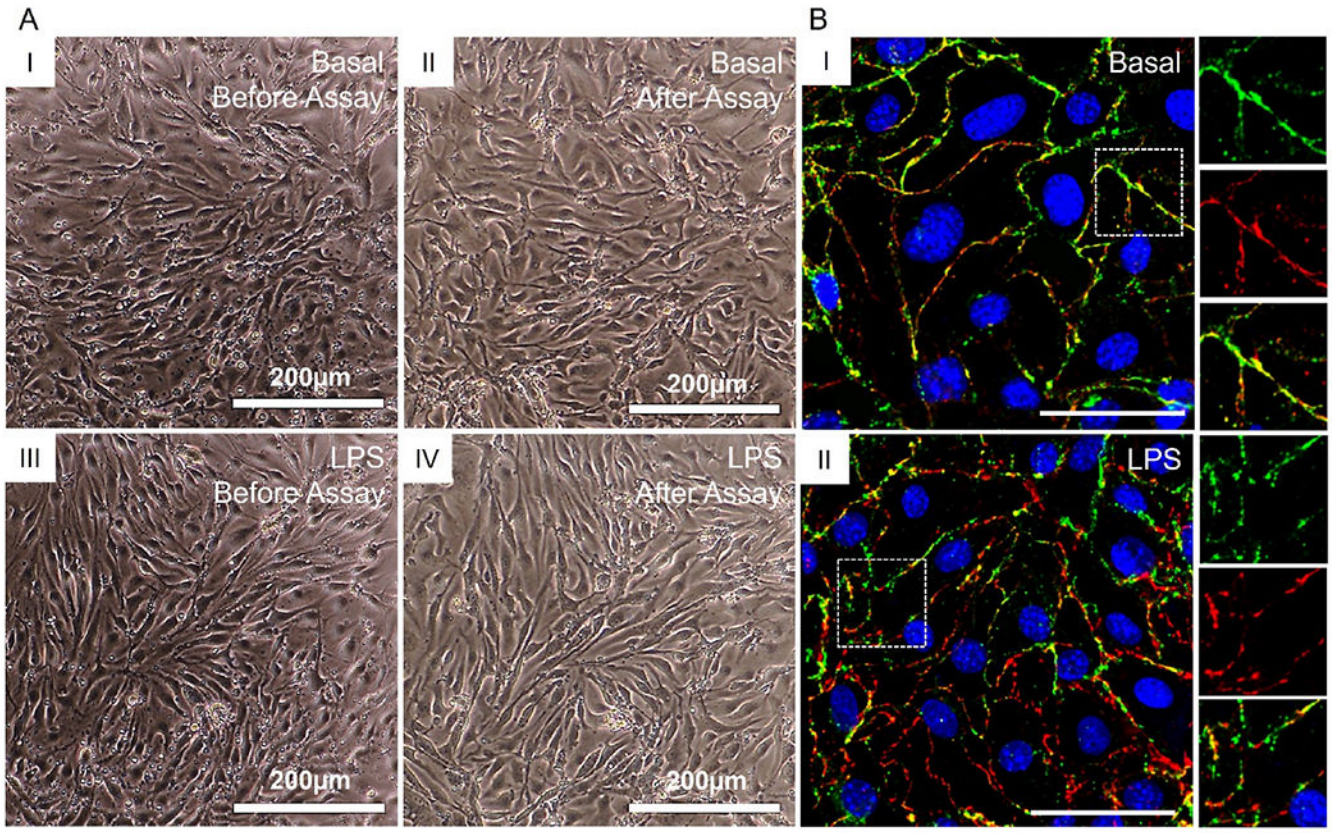

Fig. 4.

(A) Phase contrast images of cultured primary mouse brain microvascular endothelial cell (mBMEC) membrane tissues (i) Phase contrast image of basal mBMEC membrane tissue before the DigiTACK assay with no LPS stimulation and (ii) after the assay. (iii) Phase contrast image of mBMEC membrane tissues before the DigiTACK assay with LPS (500 ng/mL) stimulation and (iv) after the assay. No significant morphological alterations were observed with the mBMEC membrane tissues between before and after the assays. (B) Confocal microscopy images of mBMEC membrane tissues after the assays. Cellular immunofluorescent staining and imaging were performed after the repeated bonding and releasing of the device on the Component 2 wafer. The green, red, and blue channels correspond to Claudin-5, ZO-1 and DAPI, respectively. We observed slight defragmented staining of Claudin-5 and ZO-1 after 10 h in the LPS-treated group relative to the control group. The unlabeled scale bars are 50 μm in length. The dotted box indicates the position of a zoomed-in image. The zoomed-in images include two single-channel images and one overlayed image for better visualization of colocalization of tight junction markers.

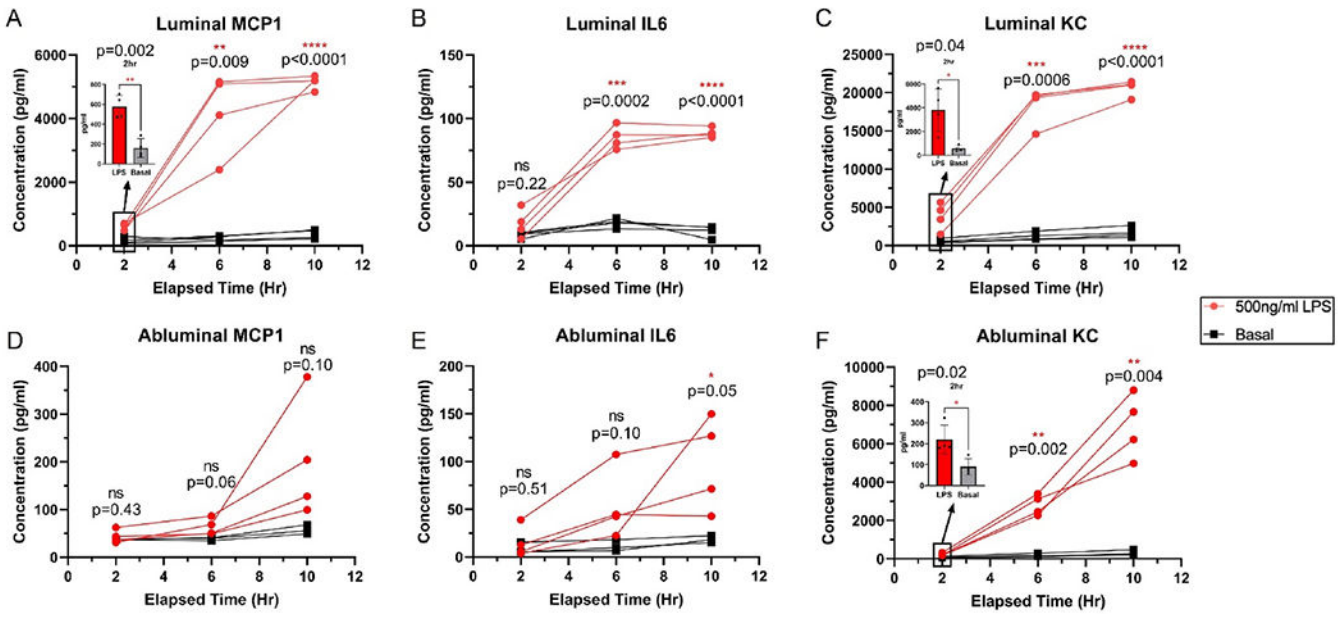

Fig. 5.

(A–F) Data from 3-plex longitudinal cytokine secretion monitoring with 8 arrayed DigiTACK devices. Each connected line represents the time variation of the measured cytokine concentration in either the luminal or abluminal compartment of each device. 4 LPS-stimulated devices and 4 basal devices were monitored for up to 10 h of stimulation/culture. The abluminal concentrations were measured with the integrated digital sensors on the Component 2 wafer. The luminal concentrations were measured from supernatants collected at each assay time point and then loaded onto the luminal measurement device. The p-values between the two conditions were calculated at each time point for all 3 markers. We were able to capture significant differences in the cytokine concentration profiles between the LPS stimulated and basal groups even at 2 h for luminal MCP1, luminal KC and abluminal KC. (p-values = 0.002, 0.04 and 0.02 respectively).